Up-Conversion Cell Imaging and pH-Induced Thermally Controlled Drug Release from $NaYF_4:Yb^{3+}/Er^{3+}$@Hydrogel Core–Shell Hybrid Microspheres

Yunlu Dai,[†,‡] Ping'an Ma,[†] Ziyong Cheng,[†,*] Xiaojiao Kang,[†,‡] Xiao Zhang,[†] Zhiyao Hou,[†] Chunxia Li,[†] Dongmei Yang,[†,‡] Xuefeng Zhai,[†] and Jun Lin[†,*]

[†]State Key Laboratory of Rare Earth Resource Utilization, Changchun Institute of Applied Chemistry, Chinese Academy of Sciences, Changchun 130022, China, and [‡]Graduate School of the Chinese Academy of Sciences, Beijing 100049, China

ABSTRACT In this study, we report a new controlled release system based on up-conversion luminescent microspheres of $NaYF_4:Yb^{3+}/Er^{3+}$ coated with the smart hydrogel poly[(*N*-isopropylacrylamide)-*co*-(methacrylic acid)] (P(NIPAM-*co*-MAA)) (prepared using 5 mol % of MAA) shell. The hybrid microspheres show bright up-conversion fluorescence under 980 nm laser excitation, and turbidity measurements show that the low critical solution temperature of the polymer shell is thermo- and pH-dependent. We have exploited the hybrid microspheres as carriers for Doxorubicin hydrochloride (DOX) due to its stimuli-responsive property as well as good biocompatibility *via* MTT assay. It is found that the drug release behavior is pH-triggered thermally sensitive. Changing the pH to mildly acidic condition at physiological temperature deforms the structure of the shell, causing the release of a large number of DOX from the microspheres. The drug-loaded microspheres exhibit an obvious cytotoxic effect on SKOV3 ovarian cancer cells. The endocytosis process of drug-loaded microspheres is observed using confocal laser scanning microscopy and up-conversion luminescence microscopy. Meanwhile, the as-prepared $NaYF_4:Yb^{3+}/Er^{3+}$@SiO_2@P(NIPAM-*co*-MAA) microspheres can be used as a luminescent probe for cell imaging. In addition, the extent of drug release can be monitored by the change of up-conversion emission intensity. These pH-induced thermally controlled drug release systems have potential to be used for *in vivo* bioimaging and cancer therapy by the pH of the microenvironment changing from 7.4 (normal physiological environment) to acidic microenvironments (such as endosome and lysosome compartments) owing to endocytosis.

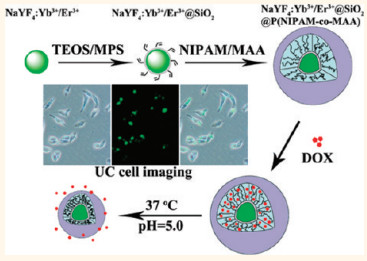

KEYWORDS: pH and temperature sensitivity · *N*-isopropylacrylamide · Doxorubicin · drug delivery · up-conversion cell imaging

In recent years, stimuli-responsive polymer materials have played an increasingly important part in a various range of applications, such as diagnostics, drug delivery, and tissue engineering, as well as biosensors and bioseparation systems.[1−8] Stimuli-responsive polymers have been designed as the multifunctional drug delivery systems (DDS), which are able to specifically accumulate in the required organ or tissue and then penetrate inside target cells, releasing the drugs.[9−12] To this end, many strategies have been developed to fabricate smart polymeric materials as drug carriers, which are responsive to a wide variety of external stimuli such as pH, temperature, light, ionic strength, and magnetic field.[13,14] Condsidering the above physiological applications, polymeric materials with both temperature and pH value response have attracted much attention. Poly(*N*-isopropylacrylamide) (PNIPAM), a commonly used thermo-responsive polymer, has a relatively low critical solution temperature (LCST) around 32−33 °C in water, which is soluble below LCST but becomes insoluble above the LCST.[15−17] Incorporating functional co-monomers into the microgels changes the LCST to higher or lower temperature, which depends on the hydrophilic or hydrophobic property of the co-monomers.[18−24]

On the other hand, lanthanide-based up-conversion fluorescent materials, which can convert longer wavelength radiation (near-infrared, NIR) to shorter wavelength fluorescence (UV or visible light) *via* a two-photon or multiphoton mechanism, have attracted a tremendous amount of attention.[25−31] Compared with conventional down-conversion fluorescent labels which require ultraviolet or blue excitation wavelength, up-conversion fluorescent materials have many conceivable advantages including greater tissue penetration, minimized autofluorescence, and high signal-to-noise ratio. Many efforts have been devoted to use up-conversion fluorescent materials in biological labeling, sensing, and imaging.[32−37]

The design of core−shell structured hybrid nanocomposites, which combine the

* Address correspondence to jlin@ciac.jl.cn, zycheng@ciac.jl.cn.

Received for review January 21, 2012 and accepted March 21, 2012.

Published online March 21, 2012
10.1021/nn300303q

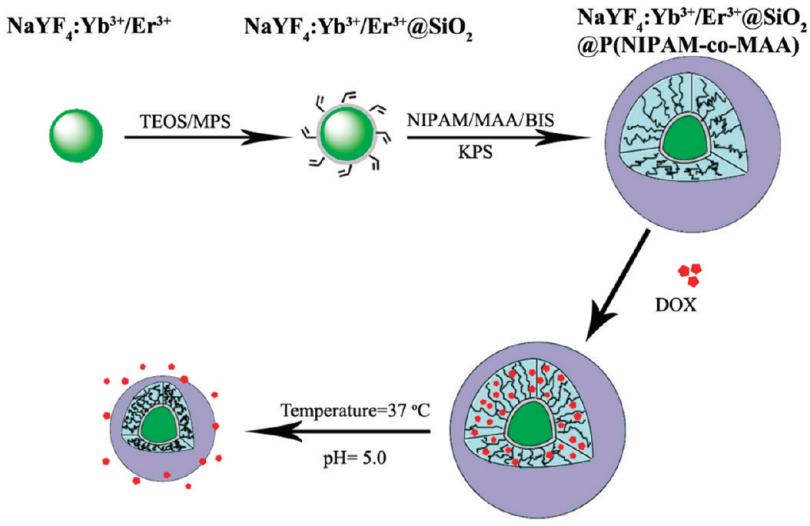

Scheme 1. Schematic illustration of the preparation process of $NaYF_4:Yb^{3+}/Er^{3+}@SiO_2@$P(NIPAM-*co*-MAA) hybrid microspheres and controlled release of DOX.

stimuli-responsive polymer and functional inorganic nanoparticles into one unit, have very promising applications in biomedical fields.[38−46] Soppimath *et al.* used pH-triggered thermally responsive P(NIPAM-*co*-*N*,*N*-dimethylacrylamide-*co*-10-undecenoic acid) as drug carriers. In an acidic environment, the LCST is below 37 °C and the particles become hydrophobic, thus leading to the release of drug molecules.[47] Xia's group has reported gold nanocages covered by P(NIPAM-*co*-acrylamide) for controlled drug release. Gold nanocages have strong absorption in the near-infrared region and convert light into heat, which rise in temperature and cause the polymer chains to collapse to release the drug in the gold nanocages.[48] Many works have focused on joining the magnetic nanoparticles and smart polymers together to form a core−shell structure for magnetic targeting and drug control and release.[49−55] Yang's group has coated P(NIPAM-*co*-*N*-hydroxymethyl acrylamide) and P(NIPAM-*co*-MAA) on magnetic mesoporous silica as a capped polymer to study drug control and release behavior.[56,57] However, as we know so far, there is no report on the combination of lanthanide-doped up-conversion luminescent materials with stimuli-responsive polymers. Recently, our group has synthesized the core−shell structured up-conversion luminescent and mesoporous $NaYF_4:Yb^{3+}/Er^{3+}@nSiO_2@mSiO_2$ microspheres, which have been attempted to be used as drug carriers to load ibuprofen (IBU).[31] Unfortunately, the rate of drug release was only governed by free diffusion, which led to a burst of drug release with about 50% IBU liberated within 5 h in simulated body fluid (SBF). The drug release profile is uncontrolled by using this kind of mesoporous silica carrier. Accordingly, in this study, we propose new inorganic−organic hybrid microspheres, which involve $NaYF_4:Yb^{3+}/Er^{3+}$ as the core and pH-induced thermo-sensitive P(NIPAM-*co*-MAA) as the shell. The obtained $NaYF_4:Yb^{3+}/Er^{3+}@SiO_2@$P(NIPAM-*co*-MAA) core/shell microspheres show bright up-conversion fluorescence under 980 nm laser excitation and were successfully applied in the imaging of cells. The hybrid microspheres can also be used as drug carriers due to their good biocompatibility *via* MTT assay. Doxorubicin hydrochloride (DOX), a well-known anticancer drug, was used as a model drug to evaluate the loading and controlled releasing behaviors of the composite microspheres. The hybrid microspheres with a smart hydrogel shell that can be rapidly collapsed when the pH of the microenvironment changes due to endocytosis from 7.4 (normal physiological environment) to acidic microenvironments (endosomes/lysosomes) could rapidly release a significant amount of DOX. The cytotoxic effect of the DOX-loaded microspheres against human SKOV3 ovarian cancer cells was examined. Meanwhile, the as-prepared $NaYF_4:Yb^{3+}/Er^{3+}@SiO_2@$P(NIPAM-*co*-MAA) microspheres can be used as excellent up-conversion luminescent probes for cell imaging, and the extent of drug release can be monitored by the up-conversion emission intensity.

RESULTS AND DISCUSSION

Preparation and Characterization of $NaYF_4:Yb^{3+}/Er^{3+}@SiO_2@$P(NIPAM-*co*-MAA). The procedure for the synthesis of $NaYF_4:Yb^{3+}/Er^{3+}@SiO_2@$P(NIPAM-*co*-MAA) is presented in Scheme 1. First, the $NaYF_4:Yb^{3+}/Er^{3+}$ microspheres were synthesized through a facile hydrothermal method. The as-prepared monodispersed $NaYF_4:Yb^{3+}/Er^{3+}$ microspheres were treated by the sol−gel process to coat them with a thin layer of silica. Then, the surface of the silica was modified with the coupling agent methacryloxypropyltrimethoxysilane (MPS), which has carbon−carbon double bonds and can react with the monomer of a

polymer in aqueous phase radical polymerization. Subsequently, the polymerization of NIPAM, MAA, and BIS on the surface of silica was carried out in deionized water.

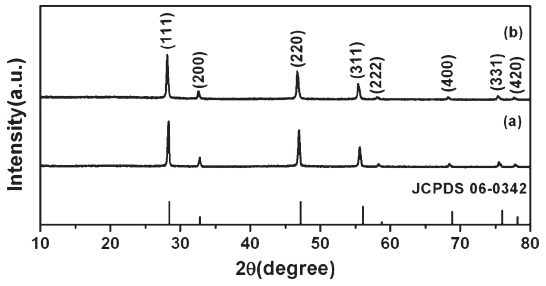

Figure 1. Wide-angle XRD patterns of the (a) $NaYF_4$:Yb^{3+}/Er^{3+}, (b) $NaYF_4$:Yb^{3+}/Er^{3+}@SiO_2 and the standard JCPDS card 06-0342 of $NaYF_4$.

Figure 1 shows the wide-angle XRD patterns of $NaYF_4$:Yb^{3+}/Er^{3+} and JCPDS card (No. 06-0342) for α-$NaYF_4$. The diffraction peaks of $NaYF_4$:Yb^{3+}/Er^{3+} from 10 to 80 ° can be indexed as the standard data (JCPDS No. 06-0342) with a space group of $Fm\bar{3}m$(225).[58] Additionally, no other peaks were found in the patterns, revealing that there is no impurity in the products.

The transmission electron microscopy (TEM) images of the core/shell structured microspheres are displayed in Figure 2. The as-synthesized $NaYF_4$:Yb^{3+}/Er^{3+} particles by a hydrothermal process consist of uniform spherical microspheres with an average diameter of 150 nm (Figure 2a,b). The obvious lattice fringes in the

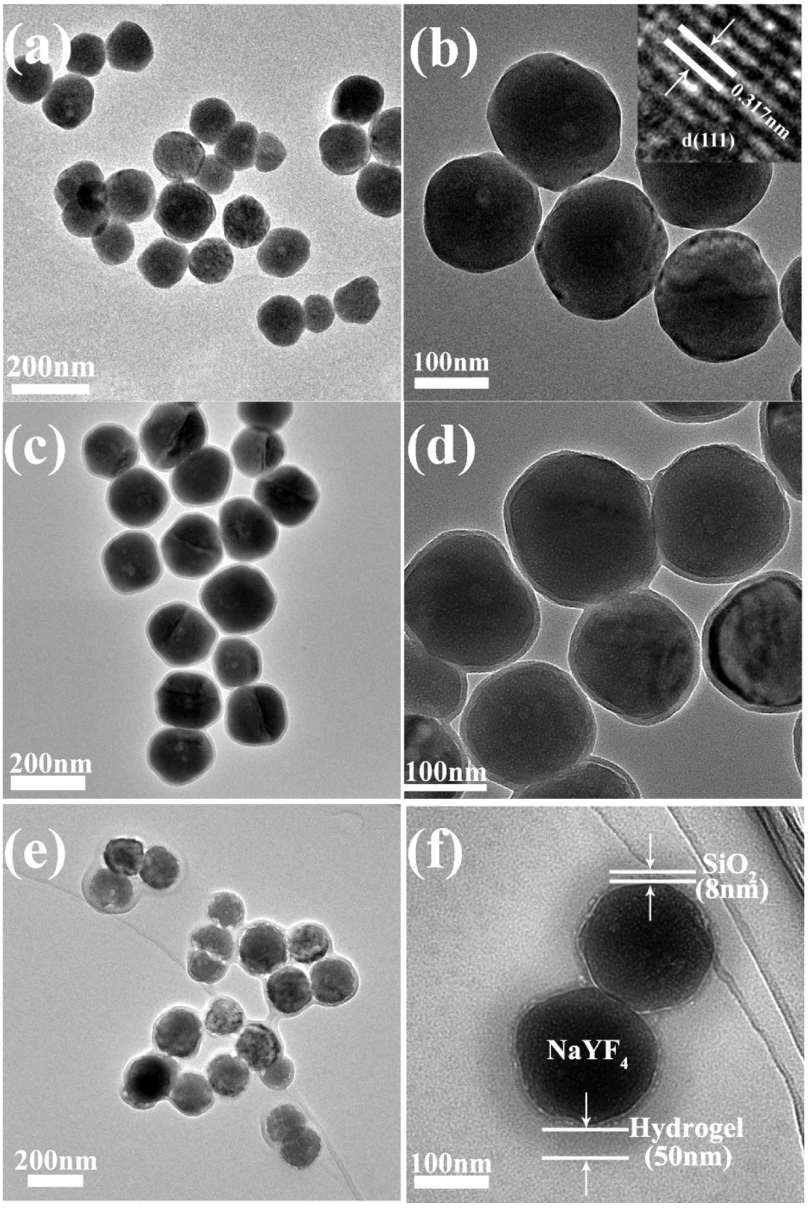

Figure 2. (a) Low- and (b) high-magnification TEM images of $NaYF_4$:Yb^{3+}/Er^{3+}, (c) low- and (d) high-magnification TEM images of $NaYF_4$:Yb^{3+}/Er^{3+}@SiO_2, (e) low- and (f) high-magnification TEM images of $NaYF_4$:Yb^{3+}/Er^{3+}@SiO_2@P(NIPAM-*co*-MAA). The inset in panel b is the HRTEM image of $NaYF_4$:Yb^{3+}/Er^{3+}.

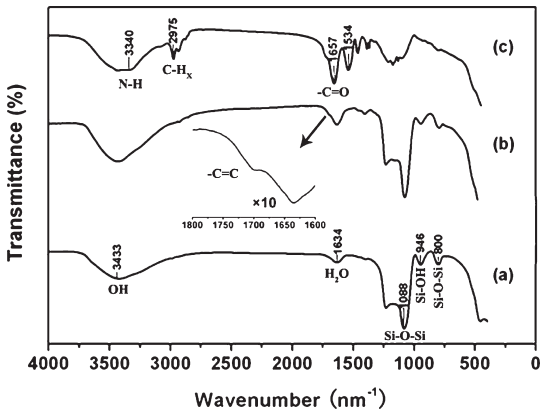

Figure 3. FTIR spectra of (a) $NaYF_4$:Yb^{3+}/Er^{3+}@SiO_2, (b) MPS modified $NaYF_4$:Yb^{3+}/Er^{3+}@SiO_2, and (c) $NaYF_4$:Yb^{3+}/Er^{3+}@SiO_2@P(NIPAM-*co*-MAA).

high-resolution transmission electron microscopy (HRTEM) images (Figure 2b, inset) confirm the high crystallinity. The interplanar distances between adjacent lattice planes (0.317 nm) is well coincident with the (111) plane of $NaYF_4$ (Figure 1). After being coated with a thin silica layer by a modified Stöber sol−gel method, $NaYF_4$:Yb^{3+}/Er^{3+}@SiO_2 microspheres still retain the morphological features of pure $NaYF_4$:Yb^{3+}/Er^{3+} and, as expected, have a uniform gray silica shell with a thickness of 8 nm (Figure 2c,d). The core/shell structure for $NaYF_4$:Yb^{3+}/Er^{3+}@SiO_2@P(NIPAM-*co*-MAA) can be seen clearly due to the different electron penetrability of the cores and polymer shells from Figure 2e,f. The average thickness of P(NIPAM-*co*-MAA) shells is 50 nm.

The FTIR spectra of $NaYF_4$:Yb^{3+}/Er^{3+}@SiO_2 (a), MPS modified $NaYF_4$:Yb^{3+}/Er^{3+}@SiO_2 (b), and $NaYF_4$:Yb^{3+}/Er^{3+}@SiO_2@P(NIPAM-*co*-MAA) (c) are shown in Figure 3. In Figure 3a, the peaks at 1088 and 800 cm^{-1} are attributed to the vibration bands of Si−O−Si, whereas the peaks at 946, 1634, and 3433 cm^{-1} belong to Si−OH, H_2O, and −OH, respectively.[57] The weak peak at 2979 cm^{-1} corresponds to $-CH_3$, which results from EDTA during the hydrothermal synthesis of $NaYF_4$:Yb, Er. After modification with MPS, the bands assigned to −C═O (1705 cm^{-1}) and $-CH_2$ (2929 cm^{-1}) are apparent (Figure 3b), which confirm the successful modification of MPS onto the surface of $NaYF_4$:Yb^{3+}/Er^{3+}@SiO_2.[59] In the spectrum of $NaYF_4$:Yb^{3+}/Er^{3+}@SiO_2@P(NIPAM-*co*-MAA) (Figure 3c), the characteristic peaks at 1657 and 1534 cm^{-1} are attributed to the secondary amide C═O stretching.[38] The peaks at 1388, 3340, and 2975 cm^{-1} belong to $-C(CH_3)_2$, N−H, and $-CH_3$, respectively. These results confirm that we have succeeded in polymerizing NIPAM and MAA onto the surface of the microspheres, which is consistent with the TEM observation. Meanwhile, the FTIR spectrum of $NaYF_4$:Yb^{3+}/Er^{3+}@SiO_2@P(NIPAM-*co*-MAA) does not show SiO_2 characteristic peaks very clearly due to large

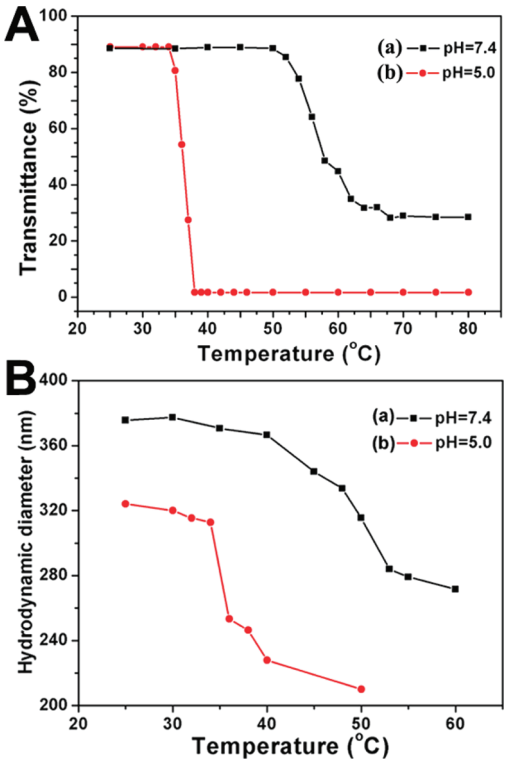

Figure 4. (A) Temperature dependence of light transmittance of $NaYF_4$:Yb^{3+}/Er^{3+}@SiO_2@P(NIPAM-*co*-MAA) solution at (a) pH = 7.4 and (b) pH = 5.0 PBS buffer at 450 nm. (B) Hydrodynamic diameter measured by DLS of $NaYF_4$:Yb^{3+}/Er^{3+}@SiO_2@P(NIPAM-*co*-MAA) solution at (a) pH = 7.4 and (b) pH = 5.0 PBS buffer.

quantities of P(NIPAM-*co*-MAA) at the surface of $NaYF_4$:Yb^{3+}/Er^{3+}@SiO_2 and a thin layer of SiO_2.

Turbidity measurements of $NaYF_4$:Yb^{3+}/Er^{3+}@SiO_2@P(NIPAM-*co*-MAA) in PBS with different pH values at 450 nm using a UV−vis spectrometer are shown in Figure 4A. At pH = 5.0, the optical transmittance exhibited no changes in the range of 25−34 °C. The transmittance decreases abruptly from 90 to 4% at 35−37 °C due to the collapse of P(NIPAM-*co*-MAA) and thereafter introducing aggregation of hybrid microspheres. We define the temperature at 50% light transmittance of the solution as LCST of the thermoresponsive polymer. So the LCST of the polymer shell is 35 °C at pH = 5.0. However, when the pH of the solution is changed to 7.4, the optical transmittance decreases slowly from 90 to 30% at 50−65 °C and the corresponding LCST of microspheres is defined to be 56 °C at pH = 7.4 PBS buffer. Moreover, dynamic light scattering (DLS) is used to further investigate the swelling/shrinking behavior of the polymer shell, and similar results were obtained with turbidity measurements. As shown in Figure 4B, the average hydrodynamic diameter of the hybrid microspheres decreases by increasing the temperature at both pH values. The hydrodynamic diameter of the hybrid microspheres at pH = 7.4 is larger than that at pH = 5.0 at the same temperature. In addition, the hydrodynamic diameter

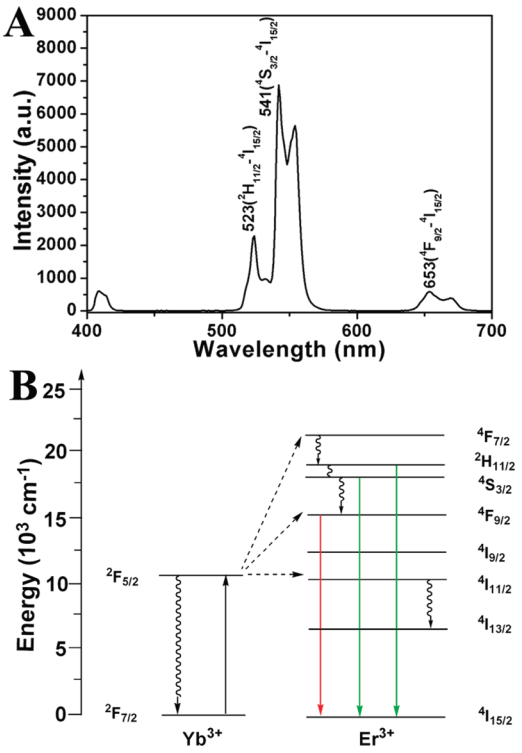

Figure 5. (A) Up-conversion emission spectra of $NaYF_4$:Yb^{3+}/Er^{3+}@SiO_2@P(NIPAM-*co*-MAA). (B) Schematic energy level diagrams, up-conversion excitation, and visible emission processes for the Yb^{3+}—Er^{3+} systems. The black, colorized, dotted arrows, and curly lines represent excitation, emission, energy transfer processes, and multiphonon relaxation, respectively.

changes greatly when the temperature changes from 34 to 36 °C at pH = 5.0. Therefore, the LCST of the polymer shell is near 35 °C at pH = 5.0 by DLS measurement, which is in good agreement with turbidity measurements (Figure 4A). However, when the pH of the solution is changed to 7.4, the hydrodynamic diameter decreases slowly below 40 °C, indicating that the LCST of the polymer shell is higher than 40 °C at pH = 7.4. As we know, PNIPAM has a LCST of around 32 °C in pure water, and the LCST can be altered by copolymerization with other functional monomers. We use 5 mol % of MAA as copolymer monomers, which change the LCST by the protonated process of carboxylic acid groups. The hybrid microspheres exhibit a pH-dependent LCST. The pK_a of PMAA is 5.5.[15] Therefore, at pH = 5.0, there are a large number of free hydrogen ions in the solution. As a result, most of the carboxylic acid groups of the PMAA are protonated due to the inter-reaction between the H^+ and the COO^-. Then, the methacrylic acid segments are relatively hydrophobic at pH = 5.0 due to protonation of the carboxylate groups, which decrease the LCST of the copolymer shell to 35 °C at pH = 5.0.[21] In contrast, at pH = 7.4, the carboxylic acid groups are essentially ionized and the hydrophilic PMAA part induces the LCST up to 56 °C. Meanwhile, the electrostatic repulsion

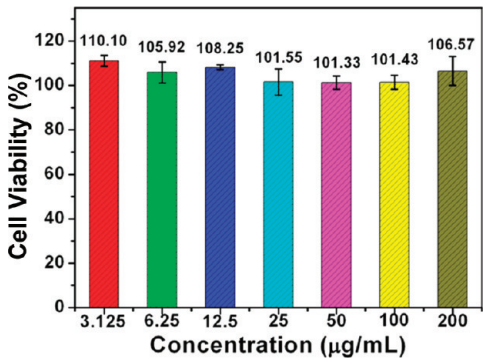

Figure 6. L929 fibroblast cell viability after incubating with $NaYF_4$:Yb^{3+}/Er^{3+}@SiO_2@P(NIPAM-*co*-MAA) microspheres for 24 h and quantitative assays by standard MTT method.

between the deprotonated carboxylic acid groups is strong, which enables the copolymer shell to swell in water.[56]

The up-conversion (UC) luminescence of rare-earth ions has been investigated extensively owing to their unique optical properties, which allow minimization of autofluorescence and photodamage as well as enable high penetration depth in tissues under a 980 nm NIR light laser excitation. In our present work, up-conversion fluorescent properties of $NaYF_4$:Yb^{3+}/Er^{3+}@SiO_2@P(NIPAM-*co*-MAA) under 980 nm excitation are shown in Figure 5A. The single emission band at 653 nm and double band at 523 and 541 nm can be assigned to $^4F_{9/2}\rightarrow{}^4I_{15/2}$, $^2H_{11/2}\rightarrow{}^4I_{15/2}$, and $^4S_{3/2}\rightarrow{}^4I_{15/2}$ transitions of Er^{3+}, respectively. The UC mechanism of Er^{3+},Yb^{3+} co-doped UC emission process is shown in Figure 5B. First, under the 980 nm NIR light, an electron of the Yb^{3+} ion is excited from the $^2F_{7/2}$ to $^2F_{5/2}$ level due to strong absorption at 980 nm of the Yb^{3+} ion. Then the electron transfers back to the ground state ($^2F_{7/2}$), while simultaneously the energy is nonradiatively transferred to Er^{3+}, resulting in a population of Er^{3+} from $^4I_{15/2}$ to $^4I_{11/2}$. A second 980 nm photon transferred by the excited Yb^{3+} ion can then populate a higher $^4F_{7/2}$ energetic state of the Er^{3+} ion, whose energy lies in the visible region. The Er^{3+} ion can then relax nonradiatively by a fast multiphonon decay process to the $^2H_{11/2}$ and $^4S_{3/2}$ levels. Finally, radiant transitions from these levels yield emissions at 523 nm ($^2H_{11/2}\rightarrow{}^4I_{15/2}$), 541 nm ($^4S_{3/2}\rightarrow{}^4I_{15/2}$), and 653 nm ($^4F_{9/2}\rightarrow{}^4I_{15/2}$).[35]

***In Vitro* Cytotoxicity and Controlled Drug Release.** To evaluate the biocompatibility of $NaYF_4$:Yb^{3+}/Er^{3+}@SiO_2@P(NIPAM-*co*-MAA) microspheres, the standard MTT cell assay was performed on L929 fibroblast cells. As shown in Figure 6, the $NaYF_4$:Yb^{3+}/Er^{3+}@SiO_2@P(NIPAM-*co*-MAA) microspheres do not show cytotoxicity against the L929 fibroblast cells. More than 100% cell viabilities were observed at a high concentration of $NaYF_4$:Yb^{3+}/Er^{3+}@SiO_2@P(NIPAM-*co*-MAA) microspheres of 200 μg/mL after incubation for 24 h. The MTT results indicate that the hybrid $NaYF_4$:Yb^{3+}/Er^{3+}@SiO_2@P(NIPAM-*co*-MAA)

microspheres have good biocompatibility as drug carriers.

We further examined the drug loading and release abilities of the $NaYF_4$:Yb^{3+}/Er^{3+}@SiO_2@P(NIPAM-*co*-MAA) hybrid microspheres. Doxorubicin hydrochloride, a commonly used chemotherapeutic drug for cancer therapy, was selected as a model drug to evaluate the loading and controlled releasing behaviors of the composite microspheres. The actual loading level of DOX in the microspheres is calculated to be 4.9% in weight, which is determined by the characteristic DOX optical absorbance at 480 nm. Figure 7A shows *in vitro* release profiles of DOX from the microspheres in PBS buffer solutions of different pH values (7.4 and 5.0) at 37 °C. Only 22% of DOX is released from the microspheres even after 72 h at pH = 7.4 and 37 °C. On the contrary, more than 90% of DOX is released within 24 h in mildly acidic conditions (pH = 5.0, 37 °C). Therefore, a pH-responsive control release system has been successfully prepared. Actually, the above release behavior can be explained by pH-induced thermally responsive P(NIPAM-*co*-MAA) shell. At pH = 7.4 and 37 °C, the LCST of polymer is 56 °C from turbidity measurement, which is just above the normal body temperature. The shells of the microspheres are hydrophilic and keep the swollen condition. Therefore, only a small quantity of DOX was leached out based on a diffusion-controlled release mechanism. However, in the mildly acidic conditions (pH = 5.0), the LCST changes to 35 °C, which is lower than the normal body temperature. The polymer shell becomes hydrophobic, which leads to the collapse and precipitation of the microspheres. Then DOX is squeezed out from the polymer shells and has a faster drug release profile. In addition, the absence of electrostatic adherence between PMAA and positive-charged DOX at pH = 5.0 might play an important role for accelerating the drug release. These results indicate that the hybrid microspheres with a pH-induced thermally responsive drug release property have potential as a smart drug carrier that can be maintained as they circulate in blood (pH = 7.4) and release DOX in mildly acidic environments (pH = 5.0) after cancer cell uptake. Meanwhile, we can monitor the cumulative release of DOX by changing the UC emission intensity of the DOX-$NaYF_4$:Yb^{3+}/Er^{3+}@SiO_2@P(NIPAM-*co*-MAA) hybrid microspheres. First, in order to exclude the dependence between the internsity of UC fluorescence and the pH value, the up-conversion fluorescence of $NaYF_4$:Yb^{3+}/Er^{3+}@SiO_2@P(NIPAM-*co*-MAA) under 980 nm excitation in PBS buffer with different pH values (7.4 and 5.0) is measured under the same condition. As shown in Figure S1 (Supporting Information), there is no obvious intensity difference between pH 7.4 and 5.0. We believe that the pH value of the solution does not affect the PL intensity of the up-conversion materials in this work. Therefore, we can monitor the

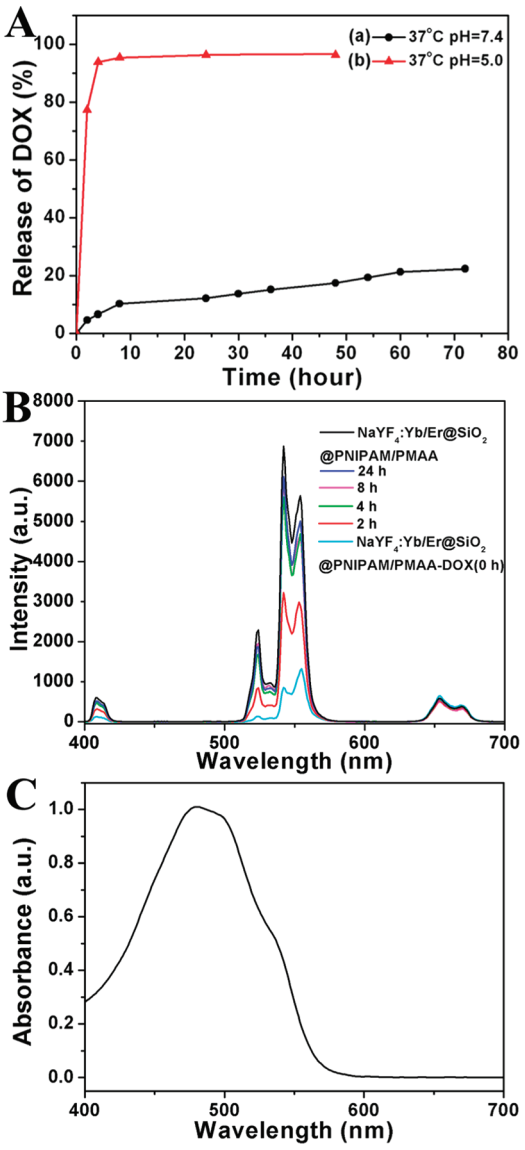

Figure 7. (A) Cumulative DOX release from $NaYF_4$:Yb^{3+}/Er^{3+}@SiO_2@P(NIPAM-*co*-MAA) at (a) pH = 7.4 and (b) pH = 5.0 PBS buffer. (B) Emission intensity of DOX-loaded $NaYF_4$:Yb,Er@SiO_2@P(NIPAM-*co*-MAA) microspheres as a function of release time at pH = 5.0 and 37 °C PBS buffer. (C) UV−vis absorption spectrum of pure DOX dissolved in PBS buffer (pH = 7.4).

cumulative release of DOX by changing the UC emission intensity of the DOX-$NaYF_4$:Yb^{3+}/Er^{3+}@SiO_2@P(NIPAM-*co*-MAA) hybrid microspheres. As given in Figure 7B, the luminescence emission intensity from 500 to 600 nm of $NaYF_4$:Yb^{3+}/Er^{3+}@SiO_2@P(NIPAM-*co*-MAA) hybrid microspheres was significantly quenched after loading DOX. In contrast, the luminescence emission intensity at 650−700 nm was unchanged. We explain the reason by the spectral overlap between UC emission of $NaYF_4$:Yb^{3+}/Er^{3+}@SiO_2@P(NIPAM-co-MAA) hybrid microspheres and absorbance of DOX. As shown in Figure 7C, the absorbance of DOX is between 400 and 580 nm, and there is no absorbance beyond 600 nm. The DOX absorption peak overlaps with the

green emission of the hybrid microspheres. Therefore, the green emission intensity of DOX-$NaYF_4$:Yb^{3+}/Er^{3+}@SiO_2@P(NIPAM-*co*-MAA) hybrid microspheres increases with the cumulative release of DOX. This allows the hybrid microspheres to be used as a bioprobe for tracking and monitoring drug release by the efficiency of UC fluorescence.

***In Vitro* Cytotoxic Effect and Cell Uptake.** To test the pharmacological activity of the DOX-loaded hybrid microspheres, the cytotoxic effect of DOX-loaded $NaYF_4$:Yb^{3+}/Er^{3+}@SiO_2@P(NIPAM-*co*-MAA) on human SKOV3 ovarian cancer cells was evaluated *in vitro via* MTT assay. Figure 8 shows the cell viabilities against free DOX, DOX-loaded $NaYF_4$:Yb^{3+}/Er^{3+}@SiO_2@P(NIPAM-*co*-MAA), and blank $NaYF_4$:Yb^{3+}/Er^{3+}@SiO_2@ P(NIPAM-*co*-MAA) at different concentrations after incubation for 48 h. It is found that the blank $NaYF_4$:Yb^{3+}/Er^{3+}@SiO_2@P(NIPAM-*co*-MAA) microspheres have no obvious cytotoxic effect on cancer cells even after 48 h treatment with the samples at a concentration as high as 200 μg/mL. The concentrations of free DOX were set to be the same as the DOX-loaded $NaYF_4$:Yb^{3+}/Er^{3+}@SiO_2@P(NIPAM-*co*-MAA). The viability of cells incubated with both free DOX and DOX-loaded $NaYF_4$:Yb^{3+}/Er^{3+}@SiO_2@P(NIPAM-*co*-MAA) decreased with increasing concentrations. At the lower concentration, free DOX exhibited a slightly higher cytotoxicity than DOX-loaded microspheres. However, the DOX-loaded microspheres exhibited similar cytotoxicity with free DOX when the concentration of DOX is up to 12.5 μg/mL. This may be attributed to the reason that small molecules like DOX can be diffused into cells rapidly whereas the microspheres have to be endocytosed to enter the cells.[60] Therefore, free DOX is faster than the DOX-loaded microspheres by cellular uptake. When the concentration is higher, more and more DOX-loaded particles can be endocytosed to enter the cancer cells and release drug inside to introduce cell death. At the cellular level, most internalization of nanoparticles will occur *via* endocytosis. After being engulfed by cells, normally the nanoparticles enter early endosomes, late endosomes, and finally fuse with lysosomes.[61] Both endosomes (pH = 5.0−6.0) and lysosomes (pH = 4.5−5.0) have an acidic microenvironment, which are distinct from the outside of the cells (pH = 7.4).[62] In addition, compared with the normal tissues, solid tumors have a weakly acidic extracellular environment of pH < 7 due to the hypoxia-induced coordinated upregulation of glycolysis.[63] It is well-known that DOX is a potent, broad-spectrum chemotherapeutic drug, which is extensively used in clinical medicine. However, it has been reported that DOX has toxic effects on normal tissues, including brain tissue and cardiac toxicity, which is even fatal in some cases.[64] In the present study, we load DOX in the pH-responsive nanocarriers, which prefer to release at the target therapy sites and can effectively decrease the side effects and toxicity of DOX.

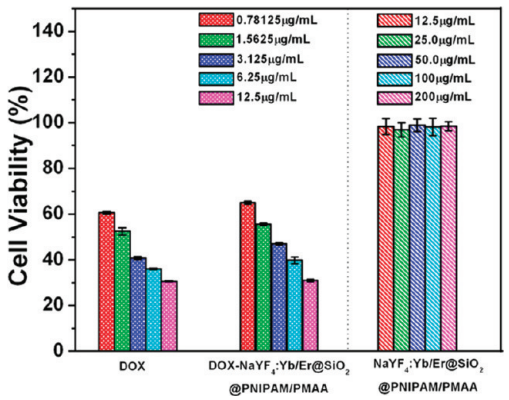

Figure 8. *In vitro* human SKOV3 ovarian cancer cell viabilities after 48 h incubation with free DOX, DOX-loaded $NaYF_4$:Yb^{3+}/Er^{3+}@SiO_2@P(NIPAM-*co*-MAA), and bare $NaYF_4$:Yb^{3+}/Er^{3+}@SiO_2@P(NIPAM-*co*-MAA) microspheres at different concentrations.

In order to further ensure the biosafety of the materials, we evaluate the cytotoxic effect of DOX-loaded $NaYF_4$:Yb^{3+}/Er^{3+}@SiO_2@P(NIPAM-*co*-MAA) on L929 fibroblast cells *in vitro via* MTT assay. Figure S2 (Supporting Information) shows the L929 fibroblast cell viabilities against free DOX, DOX-loaded $NaYF_4$:Yb^{3+}/Er^{3+}@SiO_2@P(NIPAM-*co*-MAA), and $NaYF_4$:Yb^{3+}/Er^{3+}@SiO_2@P(NIPAM-*co*-MAA) for 48 h at different concentrations. It was observed that DOX had a strong killing effect for a normal L929 cell line. However, the viability of L929 fibroblast cells is higher than that of human SKOV3 ovarian cancer cells under identical DOX concentrations (Figure 8), especially in the lower concentration, indicating that DOX has a slightly selective inhibition for cancer cells. Meanwhile, it is found that free DOX exhibited higher cytotoxicity to L929 fibroblast cells than DOX-loaded microspheres at the lower concentrations. This result suggests that DOX-loaded microspheres may reduce the side effect of DOX to normal cells at the lower concentration. In this study, DOX is absorbed and entrapped in the polymer shell, and they are expected to minimize drug release in the blood circulation (pH = 7.4) to eliminate the toxicity to normal tissues and accelerate drug release in tumor tissue. In addition, the blank $NaYF_4$:Yb^{3+}/Er^{3+}@SiO_2@P(NIPAM-*co*-MAA) microspheres have no obvious cytotoxic effect on L929 fibroblast cells even after 48 h.

To facilitate the observations of cell uptake of the microspheres, the confocal laser scanning microscopy (CLSM) photographs of human SKOV3 ovarian cancer cells incubated with DOX-loaded $NaYF_4$:Yb^{3+}/Er^{3+}@SiO_2@P(NIPAM-*co*-MAA) for 10 min, 1 h, and 6 h at 37 °C were performed, as shown in Figure 9. In the first 10 min (Figure 9a−c), only a few of microspheres could be taken up by SKOV3 cells. It is clear that the red-emitting particles accumulated near the nucleus apparently increased after incubation for 1 h (Figure 9d−f). If the

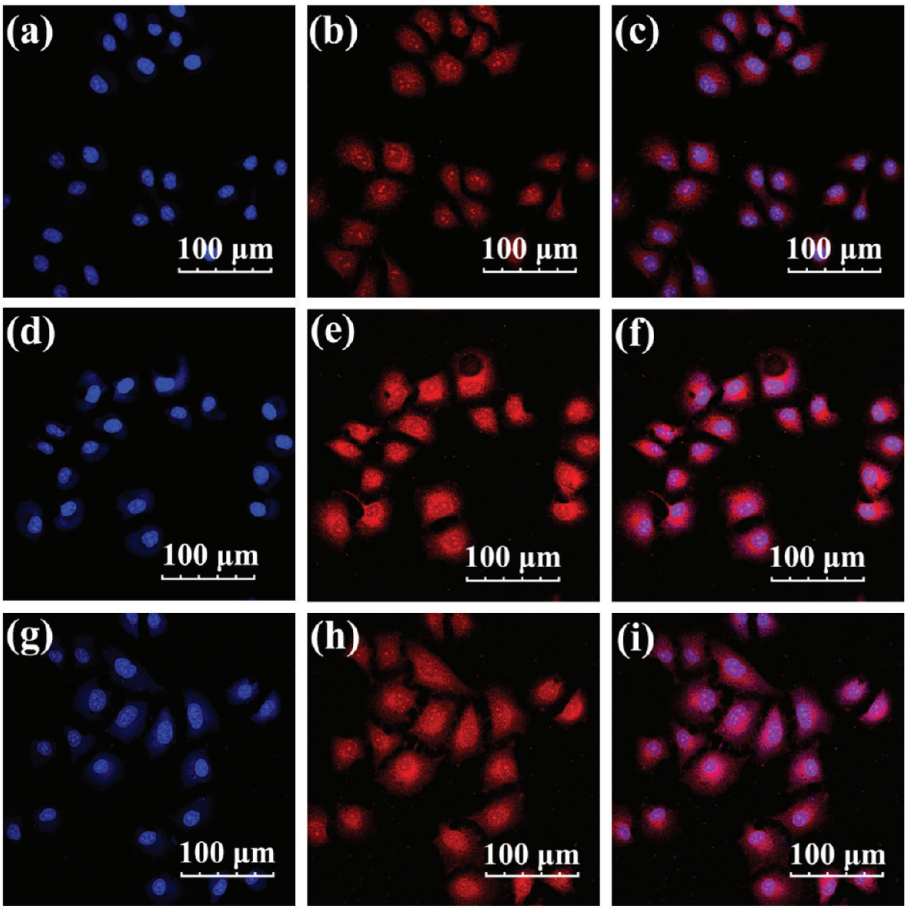

Figure 9. Confocal laser scanning microscopy (CLSM) images of human SKOV3 ovarian cancer cells incubated with DOX-loaded $NaYF_4$:Yb^{3+}/Er^{3+}@SiO_2@P(NIPAM-*co*-MAA) ([DOX] = 20 μg/mL) for 10 min (a−c), 1 h (d−f), and 6 h (g−i) at 37 °C. Each series can be classified to the nuclei of cells (being dyed in blue by Hoechst 33324 for visualization), DOX-loaded $NaYF_4$:Yb, Er@SiO_2@P(NIPAM-*co*-MAA), and a merge of the two channels of both above, respectively. The excitation wavelength of Hoechst 33342 and DOX are 405 and 543 nm, respectively.

incubation time was prolonged to 6 h (Figure 9g−i), the red fluorescence from DOX was observed in both the cytoplasm and the cell nucleus. The time course CLSM images suggest that the intracellular pathway that the DOX-loaded $NaYF_4$:Yb^{3+}/Er^{3+}@SiO_2@P(NIPAM-*co*-MAA) used to deliver DOX comprised rapid internalization, microsphere localization in the cytoplasm, and DOX localization in the cell nucleus.

Near-infrared (NIR) radiation has proven to be a promising tool for both *in vivo* imaging and photothermal cancer treatment. Within the safe power, NIR light can penetrate the human body to a high depth owing to its minimal absorbance by skin and tissue. However, commonly used NIR chromophores have certain drawbacks, such as high toxicity of quantum dots or poor stability due to photobleaching of organic dyes. Therefore, lanthanide-doped up-conversion materials have attracted a tremendous amount of attention due to their good properties including no bleaching, high stability, high signal-to-noise ratio, sharp absorption, and emission lines.[65−68] In our present work, we also used time course up-conversion luminescence microscopy (UCLM) to investigate the interaction between SKVO3 ovarian cells and the $NaYF_4$:Yb^{3+}/Er^{3+}@SiO_2@P(NIPAM-*co*-MAA) hybrid microspheres. SKVO3 ovarian cells were incubated with $NaYF_4$:Yb^{3+}/Er^{3+}@SiO_2@P(NIPAM-*co*-MAA) for 10 min, 1 h, 3 h, and 6 h at 37 °C, and the luminescence images were taken with an external 980 nm laser as the excitation source. After rinsing with abundant PBS to remove surface-attached microspheres, the cells were investigated by UCLM. The results for luminescence imaging are shown in Figure 10. We can see that the SKVO3 ovarian cells showed a bright green luminescence in the dark, which is in good agreement with the UC luminescent spectrum of $NaYF_4$:Yb^{3+}/Er^{3+}@SiO_2@P(NIPAM-*co*-MAA). Meanwhile, more and more $NaYF_4$:Yb^{3+}/Er^{3+}@SiO_2@P(NIPAM-*co*-MAA) hybrid microspheres were internalized into the cells as the time was prolonged from 10 min to 6 h. These results demonstrate that the as-prepared $NaYF_4$:Yb^{3+}/Er^{3+}@SiO_2@P(NIPAM-*co*-MAA) microspheres can be used as an excellent luminescent probe for cell imaging and monitoring the cell endocytosis process.

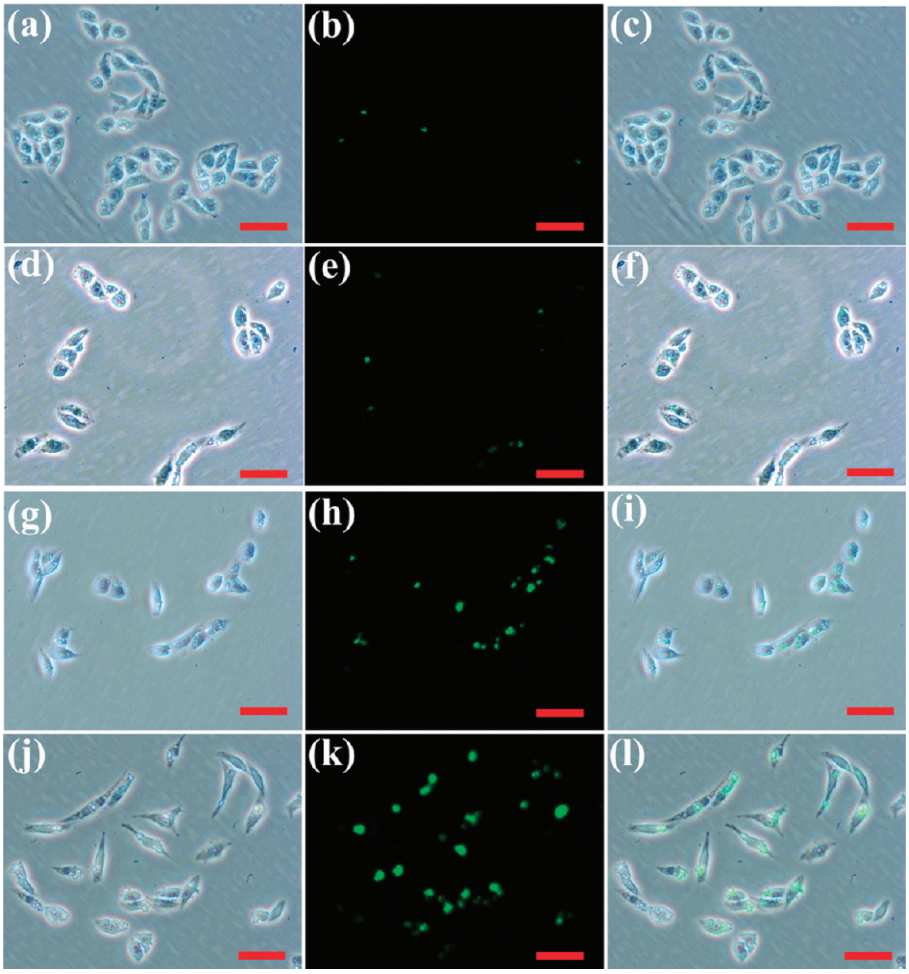

Figure 10. Inverted fluorescence microscope images of human SKOV3 ovarian cancer cells incubated with $NaYF_4:Yb^{3+}/Er^{3+}@SiO_2@P(NIPAM\text{-}co\text{-}MAA)$ for 10 min (a–c), 1 h (d–f), 3 h (g–i), and 6 h (j–l) at 37 °C. Each series can be classified to the bright-field (left column), up-conversion luminescent images (middle column) in dark-field, and overlay of both above (right column), respectively. All scale bars are 50 μm.

CONCLUSION

In summary, a new kind of core/shell $NaYF_4:Yb^{3+}/Er^{3+}@SiO_2@P(NIPAM\text{-}co\text{-}MAA)$ microsphere has been successfully prepared. The obtained core–shell structured materials have spherical morphology and narrow size distribution, which show bright up-conversion fluorescence under 980 nm laser excitation. The lower critical solution temperature (LCST) of the polymer shell was pH-dependent due to 5 mol % of PMAA copolymerization in the shell. We have exploited the hybrid microspheres as carriers for the DOX because of its good biocompatibility *via* MTT assay, and the DOX release was also pH-dependent, which can be reasoned by the change of LCST of the polymer shell. The drug-loaded microspheres exhibit an obviously cytotoxic effect on cancer cells. The endocytosis process of drug-loaded $NaYF_4:Yb^{3+}/Er^{3+}@SiO_2@P(NIPAM\text{-}co\text{-}MAA)$ by human SKOV3 ovarian cancer cells is demonstrated through confocal laser scanning microscopy photographs and up-conversion luminescence microscopy. Meanwhile, the as-prepared $NaYF_4:Yb^{3+}/Er^{3+}@SiO_2@P(NIPAM\text{-}co\text{-}MAA)$ microspheres can be used as excellent luminescent probes for up-conversion cell imaging. The above results demonstrate that this pH-induced thermally responsive controlled release system can be used as luminescent bioprobes and rapidly release the anticancer drug after endocytosis by cancer cells (pH = 5.0, 37 °C) from normal body environment (pH = 7.4, 37 °C).

MATERIALS AND METHODS

Chemicals and Materials. Y_2O_3 (99.99%), Yb_2O_3 (99.99%), and Er_2O_3 (99.99%) were purchased from Science and Technology Parent Company of the Changchun Institute of Applied Chemistry. Ethylenediaminetetraactic acid disodium salt (EDTA) (A.R.), NaF (A.R.), $K_2S_2O_8$ (A.R.), NH_4OH (25%), and isopropyl alcohol (A.R.) were purchased from Beijing Chemical Regent Co., Ltd. Methacrylic acid (MAA), *N*,*N*′-methylenebisacrylamide (BIS), and methacryloxypropyltrimethoxysilane (MPS) were obtained from Aladdin. DOX is obtained from the Nanjing Duodian Chemical Limited Company. All of the above chemicals were

used without further purification. *N*-Isopropylacrylamide (Acros Organics, 99%) was recrystallized from hexane. $Y(NO_3)_3$, $Yb(NO_3)_3$, and $Er(NO_3)_3$ stock solutions were prepared by dissolving respective rare-earth oxides in dilute HNO_3, drying at elevated temperatures to evaporate water and the excessive HNO_3, and dissolving in water.

Synthesis of $NaYF_4$:Yb^{3+}/Er^{3+}. The spherical $NaYF_4$:Yb^{3+}/Er^{3+} particles were prepared according to the literature.[69] Typically, 0.8 mmol of ethylenediaminetetraactic acid disodium salt (EDTA) was dissolved in deionized water. A total 4 mL of $Y(NO_3)_3$, $Yb(NO_3)_3$, and $Er(NO_3)_3$ (0.2 M) (lanthanide ion molar ratio, Y/Yb/Er = 80:18:2) was added into the above solution and stirred at room temperature for 1 h. Then, 12 mL of NaF aqueous solution (0.8 M) was added into the above solution and stirred for another 1 h. The as-obtained mixing solution was transferred into a Teflon bottle held in a stainless steel autoclave, sealed, and maintained at 180 °C for 2 h, and then allowed to cool to room temperature naturally. The precipitates of $NaYF_4$:Yb^{3+}/Er^{3+} in the autoclave were separated by centrifugation and washed several times with deionized water and ethanol and then dried in air at 80 °C for 12 h.

Synthesis of $NaYF_4$:Yb^{3+}/Er^{3+}@SiO_2-MPS:$NaYF_4$. Yb^{3+}/Er^{3+}@SiO_2 core/shell nanoparticles were prepared by a modified Stöber method.[70] Typically, 50 mg of $NaYF_4$:Yb^{3+}/Er^{3+}, 70 mL of isopropyl alcohol, 7.5 mL of H_2O, and 0.5 mL of NH_4OH (25%) were mixed together and stirred at room temperature for 1 h. Then, 0.05 mL of TEOS was added into the above solution and stirred for another 2 h. The product was collected by centrifugation and washed with ethanol. To functionalize the surface of $NaYF_4$:Yb^{3+}/Er^{3+}@SiO_2 microspheres, the $NaYF_4$:Yb^{3+}/Er^{3+}@SiO_2 microspheres were redispersed in 140 mL of ethanol, and 1.0 mL of MPS was added to the dispersion. After being stirred for 48 h at 30 °C, the $NaYF_4$:Yb^{3+}/Er^{3+}@SiO_2-MPS microspheres were washed with ethanol several times.

Synthesis of $NaYF_4$:Yb^{3+}/Er^{3+}@SiO_2@P(NIPAM-*co*-MAA). $NaYF_4$:Yb^{3+}/Er^{3+}@SiO_2@P(NIPAM-*co*-MAA) composites were achieved by a conventional emulsion polymerization according to the modified reported process.[71] Typically, 100 mg of $NaYF_4$:Yb^{3+}/Er^{3+}@SiO_2-MPS was dispersed in a solution containing 0.45 g of *N*-isopropylacrylamide (NIPAM), 34.07 mg of BIS, 18.78 μL of methacrylic acid (MAA), and 100 mL of deionized water. The solution was heated to 40 °C to obtain an emulsion with the protection of N_2. Then the solution was heated to 75 °C. Another solution containing 1 mg of potassium peroxodisulfate (KPS) and 1 mL of deionized water was rapidly added into the above solution. The polymerization proceeded for 4 h at 75 °C. The resulting turbid solution was then cooled to room temperature. The $NaYF_4$:Yb^{3+}/Er^{3+}@SiO_2@P(NIPAM-*co*-MAA) composites were washed with water three times.

***In Vitro* DOX Loading and Release.** Six milligrams of $NaYF_4$:Yb^{3+}/Er^{3+}@SiO_2@P(NIPAM-*co*-MAA) was dispersed in 2 mL of deionized water, and 2 mL of DOX (1 mg/mL) was added into the above solution. The mixture was shaken for 24 h at room temperature to reach the equilibrium state. Then the solution was centrifuged to collect the DOX-loaded $NaYF_4$:Yb^{3+}/Er^{3+}@SiO_2@P(NIPAM-*co*-MAA) sample. The supernatant solutions were collected, and the content of DOX was determined by UV−vis spectral measurement at the wavelength of 480 nm. DOX-loaded $NaYF_4$:Yb^{3+}/Er^{3+}@SiO_2@P(NIPAM-*co*-MAA) sample was immersed in 1 mL of phosphate buffered saline (PBS) (pH = 7.4 or 5.0) solution at 37 °C. At selected time intervals, buffer solution was taken and replaced with fresh buffer solution. The amounts of released DOX in the supernatant solutions were measured by a UV−vis spectrophotometer.

***In Vitro* Cytotoxicity of DOX-Loaded $NaYF_4$:Yb^{3+}/Er^{3+}@SiO_2@P(NIPAM-*co*-MAA) Microspheres and Cell Viability.** *In vitro* cytotoxicity of $NaYF_4$:Yb^{3+}/Er^{3+}@SiO_2@P(NIPAM-*co*-MAA) microspheres was assayed against human SKOV3 ovarian cancer cells and L929 cells. Human SKOV3 ovarian cancer cells and L929 cells were seeded in a 96-well plate at a density of 8000 cells per well and cultured in 5% CO_2 at 37 °C for 24 h. Then free DOX, DOX-loaded $NaYF_4$:Yb^{3+}/Er^{3+}@SiO_2@P(NIPAM-*co*-MAA) microspheres, and $NaYF_4$:Yb^{3+}/Er^{3+}@SiO_2@P(NIPAM-*co*-MAA) blank microspheres were added to the medium, and the cells were incubated in 5% CO_2 at 37 °C for 48 h. The concentrations of the nanospheres were 12.5, 25.0, 50.0, 100, and 200 μg/mL. The concentrations of DOX were 0.78125, 1.5625, 3.125, 6.25, and 12.5 μg/mL. At the end of the incubation, the medium containing the nanospheres was removed, and 20 μL of 3-[4,5-dimethylthiazol-2-yl]-2,5-diphenyltetrazolium bromide (MTT) solution (diluted in a culture medium with a final concentration of 0.8 mg/mL) was added into each cell and incubated for another 4 h. The supernatant in each well was aspirated. Then, 150 μL of dimethyl sulfoxide (DMSO) was added to each well before the plate was examined using a microplate reader (Therom Multiskan MK3) at the wavelength of 490 nm. Meanwhile, cell viability was also determined using MTT assay, which was the same as the procedure for cytotoxicity assay for $NaYF_4$:Yb^{3+}/Er^{3+}@SiO_2@P(NIPAM-*co*-MAA) microspheres.

Confocal Laser Scanning Microscopy (CLSM) Observation of the $NaYF_4$:Yb^{3+}/Er^{3+}@SiO_2@P(NIPAM-*co*-MAA) Microspheres. For CLSM, the SKOV3 ovarian cancer cells were seeded in 6-well culture plates (a clean coverslip was put in each well) and grown overnight as a monolayer and were incubated with DOX-loaded $NaYF_4$:Yb^{3+}/Er^{3+}@SiO_2@P(NIPAM-*co*-MAA) microspheres (DOX = 20 μg/mL) at 37 °C for different times. Thereafter, the cells were rinsed with PBS three times, fixed with 2.5% formaldehyde (1 mL/well) at 37 °C for 10 min, and then rinsed with PBS three times again. In order label the nucleus, the nuclei were stained with Hoechst 33342 solution (from Molecular Probes, 20 mg/mL in PBS, 1 mL/well) for 10 min and then rinsed with PBS three times. The coverslips were placed on a glass microscope slide, and the samples were visualized using CLSM (FV10-ASW).

Up-Conversion Luminescence Microscopy (UCLM) Observation of the $NaYF_4$:Yb^{3+}/Er^{3+}@SiO_2@P(NIPAM-*co*-MAA) Microspheres. The instrument of UCLM was rebuilt on an inverted fluorescence microscope (Nikon Ti-S), and an external CW 980 nm diode laser was illuminated onto the samples. UC luminescence (UCL) imaging of SKVO3 cells (5×10^4/well) were seeded in 6-well culture plates and grown overnight as a monolayer and were incubated with $NaYF_4$:Yb^{3+}/Er^{3+}@SiO_2@P(NIPAM-*co*-MAA) at 37 °C for a different time of 1 h. Thereafter, the cells were washed with PBS three times, fixed with 2.5% formaldehyde (1 mL/well) at 37 °C for 10 min, and then washed with PBS three times.

Characterization. The X-ray diffraction (XRD) measurements were performed on a D8 Focus diffractometer (Bruker) with Cu Kα radiation (λ = 0.15405 nm). Transmission electron microscopy (TEM) was obtained using FEI Tecnai G2 S-Twin with a field emission gun operating at 200 kV. Fourier transform infrared spectra were measured on a Vertex Perkin−Elmer 580BIR spectrophotometer (Bruker) with the KBr pellet technique. The UV−vis adsorption spectral values and light transmittance of microspheres in PBS (3 mg/mL) were measured on a Hitachi U-3100 spectrophotometer. The hydrodynamic diameter of the hybrid microspheres was measured by dynamic light scattering (DLS) using an autosizer Zen3600 (Malvern). The UC emission spectra were taken on an F-7000 spectrophotometer (Hitachi) equipped using a 980 nm laser as the excitation source. Confocal laser scanning microscopy (CLSM) images were observed by confocal laser scanning microscope (Olympus, FV 1000).

Conflict of Interest: The authors declare no competing financial interest.

Acknowledgment. This project is financially supported by National Basic Research Program of China (2010CB327704), the National Natural Science Foundation of China (NSFC 51172228, 21101149, 51172227, 20921002, 60977013), and National High Technology Research Program of China (2011AA03A407).

Supporting Information Available: The up-conversion emission spectra of $NaYF_4$:Yb^{3+}/Er^{3+}@SiO_2@P(NIPAM-*co*-MAA) under 980 nm excitation in PBS buffers with different pH values (7.4 and 5.0) (Figure S1). The MTT results of L929 cells after incubation 48 h with free DOX, DOX-loaded $NaYF_4$:Yb^{3+}/Er^{3+}@SiO_2@P(NIPAM-*co*-MAA), and bare $NaYF_4$:Yb^{3+}/Er^{3+}@SiO_2@P(NIPAM-*co*-MAA) microspheres (Figure S2). This material is available free of charge *via* the Internet at http://pubs.acs.org.

REFERENCES AND NOTES

1. Stuart, M. A. C.; Huck, W. T. S.; Genzer, J.; Muller, M.; Ober, C.; Stamm, M.; Sukhorukov, G. B.; Szleifer, I.; Tsukruk, V. V.; Urban, M.; *et al.* Emerging Applications of Stimuli-Responsive Polymer Materials. *Nat. Mater.* **2010**, *9*, 101–113.
2. Chiu, H. C.; Lin, Y. W.; Huang, Y. F.; Chuang, C. K.; Chern, C. S. Polymer Vesicles Containing Small Vesicles within Interior Aqueous Compartments and pH-Responsive Transmembrane Channels. *Angew. Chem., Int. Ed.* **2008**, *47*, 1875–1878.
3. Sinne, E. K.; Ritz, S.; Wang, Y.; Dostálek, J.; Jonas, U.; Knoll, W. Molecularly Controlled Functional Architectures. *Mater. Today* **2010**, *13*, 46–55.
4. Liu, S.-Q.; Wiradharma, N.; Gao, S.-J.; Tong, Y. W.; Yang, Y.-Y. Bio-Functional Micelles Self-Assembled from a Folate-Conjugated Block Copolymer for Targeted Intracellular Delivery of Anticancer Drugs. *Biomaterials* **2007**, *28*, 1423–1433.
5. Gong, Y.; Gao, M.; Wang, D.; Möhwald, H. Incorporating Fluorescent CdTe Nanocrystals into a Hydrogel *via* Hydrogen Bonding: Toward Fluorescent Microspheres with Temperature-Responsive Properties. *Chem. Mater.* **2005**, *17*, 2648–2653.
6. Lutolf, M. P.; Lauer-Fields, J. L.; Schmoekel, H. G.; Metters, A. T.; Weber, F. E.; Fields, G. B.; Hubbell, J. A. Synthetic Matrix Metalloproteinase-Sensitive Hydrogels for the Conduction of Tissue Regeneration: Engineering Cell-Invasion Characteristics. *Proc. Natl. Acad. Sci. U.S.A.* **2003**, *100*, 5413–5418.
7. Levy, T.; Dejugnat, C.; Sukhorukov, G. B. Polymer Microcapsules with Carbohydrate-Sensitive Properties. *Adv. Funct. Mater.* **2008**, *18*, 1586–1594.
8. Liu, S. Q.; Tong, Y. W.; Yang, Y.-Y. Incorporation and *In Vitro* Release of Doxorubicin in Thermally Sensitive Micelles Made from Poly(*N*-isopropylacrylamide-*co*-*N*,*N*-dimethylacrylamide)-*b*-Poly(D,L-lactide-*co*-glycolide) with Varying Compositions. *Biomaterials* **2005**, *26*, 5064–5074.
9. Xu, F. J.; Kang, E. T.; Neoh, K. G. pH- and Temperature-Responsive Hydrogels from Crosslinked Triblock Copolymers Prepared *via* Consecutive Atom Transfer Radical Polymerizations. *Biomaterials* **2006**, *27*, 2787–2797.
10. Deka, S. R.; Quarta, A.; Di Corato, R.; Riedinger, A.; Cingolani, R.; Pellegrino, T. Magnetic Nanobeads Decorated by Thermo-Responsive PNIPAM Shell as Medical Platforms for the Efficient Delivery of Doxorubicin to Tumour Cells. *Nanoscale* **2011**, *3*, 619–629.
11. Chen, Y.; Chen, H. R.; Zeng, D. P.; Tian, Y. B.; Chen, F.; Feng, J. W.; Shi, J. L. Core/Shell Structured Hollow Mesoporous Nanocapsules: A Potential Platform for Simultaneous Cell Imaging and Anticancer Drug Delivery. *ACS Nano* **2010**, *4*, 6001–6013.
12. Guo, J.; Yang, W. L.; Wang, C. C.; He, J.; Chen, J. Y. Poly(*N*-isopropylacrylamide)-Coated Luminescent/Magnetic Silica Microspheres: Preparation, Characterization, and Biomedical Applications. *Chem. Mater.* **2006**, *18*, 5554–5562.
13. De Geest, B. G.; Sanders, N. N.; Sukhorukov, G. B.; Demeester, J.; De Smedt, S. C. Release Mechanisms for Polyelectrolyte Capsules. *Chem. Soc. Rev.* **2007**, *36*, 636–649.
14. Delcea, M.; Möhwald, H.; Skirtach, A. G. Stimuli-Responsive LbL Capsules and Nanoshells for Drug Delivery. *Adv. Drug Delivery Rev.* **2011**, *63*, 730–747.
15. Grimshaw, P. E.; Nussbaum, J. H.; Grodzinsky, A. J.; Yarmush, M. L. Kinetics of Electrically and Chemically-Induced Swelling in Polyelectrolyte Gels. *J. Chem. Phys.* **1990**, *93*, 4462–4472.
16. Lu, Y.; Yuan, J. Y.; Polzer, F.; Drechsler, M.; Preussners, J. *In Situ* Growth of Catalytic Active Au–Pt Bimetallic Nanorods in Thermoresponsive Core–Shell Microgels. *ACS Nano* **2010**, *4*, 7078–7086.
17. Lo, C.-L.; Huang, C.-K.; Lin, K.-M.; Hsiue, G.-H. Mixed Micelles Formed from Graft and Diblock Copolymers for Application in Intracellular Drug Delivery. *Biomaterials* **2007**, *28*, 1225–1235.
18. Deng, Y. H.; Yang, W. L.; Wang, C. C.; Fu, S. K. A Novel Approach for Preparation of Thermoresponsive Polymer Magnetic Microspheres with Core–Shell Structure. *Adv. Mater.* **2003**, *15*, 1729–1732.
19. Weng, Y.; Ding, Y.; Zhang, G. Microcalorimetric Investigation on the Lower Critical Solution Temperature Behavior of *N*-Isopropycrylamide-*co*-Acrylic Acid Copolymer in Aqueous Solution. *J. Phys. Chem. B* **2006**, *110*, 11813–11817.
20. Saunders, B. R.; Crowther, H. M.; Vincent, B. Poly(methyl methacrylate)-*co*-(methacrylic acid) Microgel Particles: Swelling Control Using pH, Cononsolvency, and Osmotic Deswelling. *Macromolecules* **1997**, *30*, 482–487.
21. Schilli, C. M.; Zhang, M. F.; Rizzardo, E.; Thang, S. H.; Chong, Y. K.; Edwards, K.; Karlsson, G.; Muller, A. H. E. A New Double-Responsive Block Copolymer Synthesized *via* RAFT Polymerization: Poly(*N*-isopropylacrylamide)-*block*-Poly(acrylic acid). *Macromolecules* **2004**, *37*, 7861–7866.
22. Pelton, R. H.; Chibante, P. Preparation of Aqueous of Aqueous Lattices with *N*-Isopropylacrylamide. *Colloids Surf.* **1986**, *20*, 247–256.
23. Pelton, R. Temperature-Sensitive Aqueous Microgels. *Adv. Colloid Interface Sci.* **2000**, *85*, 1–33.
24. Hoare, T.; Pelton, R. Calorimetric Analysis of Thermal Phase Transitions in Functionalized Microgels. *J. Phys. Chem. B* **2007**, *111*, 1334–1342.
25. Wang, M.; Mi, C.-C.; Wang, W.-X.; Liu, C.-H.; Wu, Y.-F.; Xu, Z.-R.; Mao, C.-B.; Xu, S.-K. Immunolabeling and NIR-Excited Fluorescent Imaging of HeLa Cells by Using $NaYF_4$:Yb,Er Upconversion Nanoparticles. *ACS Nano* **2009**, *3*, 1580–1586.
26. Li, Z.; Zhang, Y.; Jiang, S. Multicolor Core/Shell-Structured Upconversion Fluorescent Nanoparticles. *Adv. Mater.* **2008**, *20*, 4765–4769.
27. Liu, Y. S.; Tu, D. T.; Zhu, H. M.; Li, R. F.; Luo, W. Q.; Chen, X. Y. A Strategy to Achieve Efficient Dual-Mode Luminescence of Eu^{3+} in Lanthanides Doped Multifunctional $NaGdF_4$ Nanocrystals. *Adv. Mater.* **2010**, *22*, 3266–3271.
28. Sharma, A. K.; Son, K. H.; Han, B. Y.; Sohn, K.-S. Simultaneous Optimization of Luminance and Color Chromaticity of Phosphors Using a Nondominated Sorting Genetic Algorithm. *Adv. Funct. Mater.* **2010**, *20*, 1750–1755.
29. Wang, F.; Wang, J.; Liu, X. Direct Evidence of a Surface Quenching Effect on Size-Dependent Luminescence of Upconversion Nanoparticles. *Angew. Chem., Int. Ed.* **2010**, *49*, 7456–7460.
30. Wang, J.; Tanner, P. A. Upconversion for White Light Generation by a Single Compound. *J. Am. Chem. Soc.* **2009**, *132*, 947–949.
31. Kang, X.; Cheng, Z.; Li, C.; Yang, D.; Shang, M.; Ma, P.; Li, G.; Liu, N.; Lin, J. Core–Shell Structured Up-Conversion Luminescent and Mesoporous $NaYF_4$:Yb^{3+}/Er^{3+}@*n*SiO_2@*m*SiO_2 Nanospheres as Carriers for Drug Delivery. *J. Phys. Chem. C* **2011**, *115*, 15801–15811.
32. Xiong, L. Q.; Yang, T. S.; Yang, Y.; Xu, C. J.; Li, F. Y. Long-Term *In Vivo* Biodistribution Imaging and Toxicity of Polyacrylic Acid-Coated Upconversion Nanophosphors. *Biomaterials* **2010**, *31*, 7078–7085.
33. Cheung, E. N. M.; Alvares, R. D. A.; Oakden, W.; Chaudhary, R.; Hill, M. L.; Pichaandi, J.; Mo, G. C. H.; Yip, C.; Macdonald, P. M.; Stanisz, G. J.; *et al.* Polymer-Stabilized Lanthanide Fluoride Nanoparticle Aggregates as Contrast Agents for Magnetic Resonance Imaging and Computed Tomography. *Chem. Mater.* **2010**, *22*, 4728–4739.
34. Yang, J. P.; Deng, Y. H.; Wu, Q. L.; Zhou, J.; Bao, H. F.; Li, Q.; Zhang, F.; Li, F. Y.; Tu, B.; Zhao, D. Y. Mesoporous Silica Encapsulating Upconversion Luminescence Rare-Earth Fluoride Nanorods for Secondary Excitation. *Langmuir* **2010**, *26*, 8850–8856.
35. Boyer, J. C.; van Veggel, F. Absolute Quantum Yield Measurements of Colloidal $NaYF_4$: Er^{3+},Yb^{3+} Upconverting Nanoparticles. *Nanoscale* **2010**, *2*, 1417–1419.
36. Quan, Z. W.; Fang, J. Y. Superlattices with Non-Spherical Building Blocks. *Nano Today* **2010**, *5*, 390–411.
37. Tu, D.; Liu, L.; Ju, Q.; Liu, Y.; Zhu, H.; Li, R.; Chen, X. Time-Resolved FRET Biosensor Based on Amine-Functionalized Lanthanide-Doped $NaYF_4$ Nanocrystals. *Angew. Chem., Int. Ed.* **2011**, *50*, 6306–6310.

38. Wu, T.; Zhang, Y. F.; Wang, X. F.; Liu, S. Y. Fabrication of Hybrid Silica Nanoparticles Densely Grafted with Thermoresponsive Poly(*N*-isopropylacrylamide) Brushes of Controlled Thickness *via* Surface-Initiated Atom Transfer Radical Polymerization. *Chem. Mater.* **2008**, *20*, 101–109.
39. Guo, J.; Wang, C. C.; Mao, W. Y.; Yang, W. L.; Liu, C. J.; Chen, J. Y. Facile One-Pot Preparation and Functionalization of Luminescent Chitosan-Poly(methacrylic acid) Microspheres Based on Polymer–Monomer Pairs. *Nanotechnology* **2008**, *19*, 315605.
40. Yang, J. X.; Hu, D. D.; Fang, Y.; Bai, C. L.; Wang, H. Y. Novel Method for Preparation of Structural Microspheres Poly(*N*-isopropylacrylamide-*co*-acrylic acid)/SiO_2. *Chem. Mater.* **2006**, *18*, 4902–4907.
41. Bikram, M.; Gobin, A. M.; Whitmire, R. E.; West, J. L. Temperature-Sensitive Hydrogels with SiO_2–Au Nanoshells for Controlled Drug Delivery. *J. Controlled Release* **2007**, *123*, 219–227.
42. Karg, M.; Hellweg, T. Smart Inorganic/Organic Hybrid Microgels: Synthesis and Characterisation. *J. Mater. Chem.* **2009**, *19*, 8714–8727.
43. Zhang, F.; Wang, C. C. Preparation of P(NIPAM-*co*-AA) Microcontainers Surface-Anchored with Magnetic Nanoparticles. *Langmuir* **2009**, *25*, 8255–8262.
44. Yang, Y.; Yan, X.; Cui, Y.; He, Q.; Li, D.; Wang, A.; Fei, J.; Li, J. Preparation of Polymer-Coated Mesoporous Silica Nanoparticles Used for Cellular Imaging by a "graft-from" Method. *J. Mater. Chem.* **2008**, *18*, 5731–5737.
45. Wu, T.; Zou, G.; Hu, J. M.; Liu, S. Y. Fabrication of Photoswitchable and Thermotunable Multicolor Fluorescent Hybrid Silica Nanoparticles Coated with Dye-Labeled Poly(*N*-isopropylacrylamide) Brushes. *Chem. Mater.* **2009**, *21*, 3788–3798.
46. Brites, C. D. S.; Lima, P. P.; Silva, N. J. O.; Millan, A.; Amaral, V. S.; Palacio, F.; Carlos, L. D. Lanthanide-Based Luminescent Molecular Thermometers. *New J. Chem.* **2011**, *35*, 1177–1183.
47. Soppimath, K. S.; Tan, D. C. W.; Yang, Y. Y. pH-Triggered Thermally Responsive Polymer Core–Shell Nanoparticles for Drug Delivery. *Adv. Mater.* **2005**, *17*, 318–323.
48. Yavuz, M. S.; Cheng, Y.; Chen, J.; Cobley, C. M.; Zhang, Q.; Rycenga, M.; Xie, J.; Kim, C.; Song, K. H.; Schwartz, A. G.; *et al.* Gold Nanocages Covered by Smart Polymers for Controlled Release with Near-Infrared Light. *Nat. Mater.* **2009**, *8*, 935–939.
49. Paquet, C.; de Haan, H. W.; Leek, D. M.; Lin, H.-Y.; Xiang, B.; Tian, G.; Kell, A.; Simard, B. Clusters of Superparamagnetic Iron Oxide Nanoparticles Encapsulated in a Hydrogel: A Particle Architecture Generating a Synergistic Enhancement of the T_2 Relaxation. *ACS Nano* **2011**, *5*, 3104–3112.
50. Purushotham, S.; Ramanujan, R. V. Thermoresponsive Magnetic Composite Nanomaterials for Multimodal Cancer Therapy. *Acta Biomater.* **2010**, *6*, 502–510.
51. Herrera, A. P.; Rodriguez, M.; Torres-Lugo, M.; Rinaldi, C. Multifunctional Magnetite Nanoparticles Coated with Fluorescent Thermo-Responsive Polymeric Shells. *J. Mater. Chem.* **2008**, *18*, 855–858.
52. Nash, M. A.; Lai, J. J.; Hoffman, A. S.; Yager, P.; Stayton, P. S. "Smart" Diblock Copolymers as Templates for Magnetic-Core Gold-Shell Nanoparticle Synthesis. *Nano Lett.* **2010**, *10*, 85–91.
53. Purushotham, S.; Chang, P. E. J.; Rumpel, H.; Kee, I. H. C.; Ng, R. T. H.; Chow, P. K. H.; Tan, C. K.; Ramanujan, R. V. Thermoresponsive Core–Shell Magnetic Nanoparticles for Combined Modalities of Cancer Therapy. *Nanotechnology* **2009**, *20*, 305101.
54. Chen, L. B.; Zhang, F.; Wang, C. C. Rational Synthesis of Magnetic Thermosensitive Microcontainers as Targeting Drug Carriers. *Small* **2009**, *5*, 621–628.
55. Parab, H. J.; Huang, J. H.; Lai, T. C.; Jan, Y. H.; Liu, R. H.; Wang, J. L.; Hsiao, M; Chen, C. H.; Hwu, Y. K.; Tsai, D. P.; *et al.* Biocompatible Transferrin-Conjugated Sodium Hexametaphosphate-Stabilized Gold Nanoparticles: Synthesis, Characterization, Cytotoxicity and Cellular Uptake. *Nanotechnology* **2011**, *22*, 395706.
56. Chang, B.; Sha, X.; Guo, J.; Jiao, Y.; Wang, C.; Yang, W. Thermo and pH Dual Responsive, Polymer Shell Coated, Magnetic Mesoporous Silica Nanoparticles for Controlled Drug Release. *J. Mater. Chem.* **2011**, *21*, 9239–9247.
57. Liu, C.; Guo, J.; Yang, W.; Hu, J.; Wang, C.; Fu, S. Magnetic Mesoporous Silica Microspheres with Thermo-Sensitive Polymer Shell for Controlled Drug Release. *J. Mater. Chem.* **2009**, *19*, 4764–4770.
58. Mai, H. X.; Zhang, Y. W.; Si, R.; Yan, Z. G.; Sun, L. D.; You, L. P.; Yan, C. H. High-Quality Sodium Rare-Earth Fluoride Nanocrystals: Controlled Synthesis and Optical Properties. *J. Am. Chem. Soc.* **2006**, *128*, 6426–6436.
59. Chen, H. M.; Deng, C. H.; Zhang, X. M. Synthesis of Fe_3O_4@SiO_2@PMMA Core–Shell–Shell Magnetic Microspheres for Highly Efficient Enrichment of Peptides and Proteins for MALDI-ToF MS Analysis. *Angew. Chem., Int. Ed.* **2010**, *49*, 607–611.
60. Chen, J.; Qiu, X.; Ouyang, J.; Kong, J.; Zhong, W.; Xing, M. M. Q. pH and Reduction Dual-Sensitive Copolymeric Micelles for Intracellular Doxorubicin Delivery. *Biomacromolecules* **2011**, *12*, 3601–3611.
61. Moore, M. N. Do Nanoparticles Present Ecotoxicological Risks for the Health of the Aquatic Environment? *Environ. Int.* **2006**, *32*, 967–976.
62. Mellman, I.; Fuchs, R.; Helenius, A. Acidification of the Endocytic and Exocytic Pathways. *Annu. Rev. Biochem.* **1986**, *55*, 663–700.
63. Stubbs, M.; McSheehy, P. M. J.; Griffiths, J. R.; Bashford, C. L. Causes and Consequences of Tumour Acidity and Implications for Treatment. *Mol. Med. Today* **2000**, *6*, 15–19.
64. Tangpong, J.; Miriyala, S.; Noel, T.; Sinthupibulyakit, C.; Jungsuwadee, P.; St. Clair, D. K. Doxorubicin-Induced Central Nervous System Toxicity and Protection by Xanthone Derivative of Garcinia Mangostana. *Neuroscience* **2011**, *175*, 292–299.
65. Jin, J.; Gu, Y.-J.; Man, C. W.-Y.; Cheng, J.; Xu, Z.; Zhang, Y.; Wang, H.; Lee, V. H.-Y.; Cheng, S. H.; Wong, W.-T. Polymer-Coated $NaYF_4$:Yb^{3+},Er^{3+} Upconversion Nanoparticles for Charge-Dependent Cellular Imaging. *ACS Nano* **2011**, *5*, 7838–7847.
66. Wang, Z.-L.; Hao, J.; Chan, H. L. W.; Law, G.-L.; Wong, W.-T.; Wong, K.-L.; Murphy, M. B.; Su, T.; Zhang, Z. H.; Zeng, S. Q. Simultaneous Synthesis and Functionalization of Water-Soluble Up-Conversion Nanoparticles for *In-Vitro* Cell and Nude Mouse Imaging. *Nanoscale* **2011**, *3*, 2175–2181.
67. Wang, C.; Tao, H.; Cheng, L.; Liu, Z. Near-Infrared Light Induced *In Vivo* Photodynamic Therapy of Cancer Based on Upconversion Nanoparticles. *Biomaterials* **2011**, *32*, 6145–6154.
68. Zhou, J.; Sun, Y.; Du, X.; Xiong, L.; Hu, H.; Li, F. Dual-Modality *In Vivo* Imaging Using Rare-Earth Nanocrystals with Near-Infrared to Near-Infrared (NIR-to-NIR) Upconversion Luminescence and Magnetic Resonance Properties. *Biomaterials* **2010**, *31*, 3287–3295.
69. Sun, Y. J.; Chen, Y.; Tian, L. J.; Yu, Y.; Kong, X. G.; Zhao, J. W.; Zhang, H. Controlled Synthesis and Morphology Dependent Upconversion Luminescence of $NaYF_4$: Yb, Er Nanocrystals. *Nanotechnology* **2007**, *18*, 275609.
70. Stober, W.; Fink, A.; Bohn, E. Controlled Growth of Monodisperse Silica Spheres in Micron Size Range. *J. Colloid Interface Sci.* **1968**, *26*, 62–69.
71. Karg, M.; Pastoriza-Santos, I.; Liz-Marzán, L. M.; Hellweg, T. A Versatile Approach for the Preparation of Thermosensitive PNIPAM Core–Shell Microgels with Nanoparticle Cores. *ChemPhysChem* **2006**, *7*, 2298–2301.